Green Chemistry

PAPER

View Article Online
View Journal

Cite this: DOI: 10.1039/c4gc01779j

Efficient and selective conversion of lactic acid into acetaldehyde using a mesoporous aluminum phosphate catalyst†

Congming Tang,*[a] Jiansheng Peng,[a] Xinli Li,[a] Zhanjie Zhai,[a] Wei Bai,[b] Ning Jiang,[b] Hejun Gao[a] and Yunwen Liao[a]

Received 14th September 2014,
Accepted 28th October 2014

DOI: 10.1039/c4gc01779j

www.rsc.org/greenchem

Although acetaldehyde is a very important compound and has been utilized as a useful synthon for various important chemicals, it has been synthesized in industry through a petroleum route until now. Herein, we have successfully developed a sustainable route using a heterogeneous catalyst. In the presence of mesoporous aluminum phosphate (MAP3), the decarbonylation reaction of lactic acid proceeded efficiently, with 100% lactic acid conversion and ~92% acetaldehyde selectivity. The catalyst shows high stability for at least 248 h. The unprecedented catalytic performance is due to rich medium acidic sites existing on the catalyst surface.

Introduction

With the increasing shortage of fossil resources, it is indispensable to develop alternative routes to synthesize bulk chemicals from non-fossil resources.[1–3] Production of bulk chemicals from bioresources is generally viewed as a promising route.[4–12] Acetaldehyde as an important chemical is widely used for the production of peracetic acid, pentaerythritol, pyridine bases, butyleneglycol, and chloral.[13,14] At present, acetaldehyde is produced by the Wacker process in which ethylene is used as the raw material, and $PdCl_2$–$CuCl_2$ is utilized as the catalytic system. Due to the increasing depletion of petroleum reserves which are used to produce ethylene *via* high temperature pyrolysis or catalytic cracking, this route will be restricted in the near future. For this reason, significant research is focused on production of acetaldehyde from biomass. A case in point is that acetaldehyde is produced *via* catalytic dehydrogenation of ethanol or partial oxidation of ethanol.[13,15–19] Acetaldehyde can also be obtained through decarbonylation of biolactic acid (LA) accompanied by formation of the by-product carbon monoxide.[20] However, carbon monoxide is easily separated from the mixtures composed of product and unreacted reagent, and can be further used to synthesize carbonyl compounds such as acetic acid, acrylic acid, and other α,β-unsaturated acids *via* carbonylation reaction of the corresponding substrates.[21–25] Carbon monoxide is also used to synthesize propionaldehyde and other aldehydes *via* hydroformylation reaction of ethylene and other alkenes.[26–29] Generally, LA is used as a crucial platform molecule which can be converted to many value added chemicals such as acrylic acid,[30–32] acetaldehyde,[20] 2,3-pentanedione,[33,34] propionic acid,[35] pyruvic acid[36] and polylactic acid.[37] To our delight, the technologies on lactic acid synthesis have made much progress and a wide range of low-cost biomass materials such as cellulose,[8] sugars,[38] and sorbitol[39] have also been used to produce LA.

Few research studies on decarbonylation of LA to acetaldehyde have been reported so far. Katryniok *et al.*[20] reported silica supported heteropolyacids for the catalytic decarbonylation of LA to acetaldehyde, achieving 91% conversion of LA as well as 81–83% yield of acetaldehyde at 275 °C. More recently, we have reported metal sulphates as catalysts for the decarbonylation of LA to acetaldehyde.[40] Under the optimal reaction conditions, the acetaldehyde yield attains 92.1% at 380 °C. Although the reported catalysts have a poor durability, the acetaldehyde yield is acceptable. The selective conversion of LA into acetaldehyde catalyzed by medium acidity has been recognized.[40] Strong acidity does not favor the decarbonylation of LA to acetaldehyde, but easily leads to the carbon deposition or coke formation causing deactivation of the catalyst.

In this work, we present an efficient and durable mesoporous aluminum phosphate catalyst for decarbonylation of LA into acetaldehyde. 100% LA conversion with ~92% acetaldehyde selectivity has been achieved over the mesoporous aluminum phosphate at 325 °C. The catalyst shows high stability for at least 248 h (Fig. 8).

[a]*Chemical Synthesis and Pollution Control Key Laboratory of Sichuan Province, China West Normal University, Nanchong, Sichuan 637002, PR China. E-mail: tcmtang2001@163.com*
[b]*Chengdu Institute of Organic Chemistry, Chinese Academy of Sciences, Chengdu, Sichuan 610041, PR China*
† Electronic supplementary information (ESI) available. See DOI: 10.1039/c4gc01779j

Results and discussion

Characterization

BET and NH_3-TPD. It is known that specific surface area is a pivotal factor for a heterogeneous catalyst since the catalytic reaction occurs on the surface of the catalyst. Besides, internal diffusion is also an important factor for the reaction rate. Therefore the specific surface area and pore structure are explored and the results are shown in Table 1. The N_2 adsorption–desorption isotherm curves for catalysts and the corresponding pore size distribution curves for catalysts are given in Fig. S1 and S2.† From the data given in Table 1, we can clearly see that specific surface areas of catalysts prepared by different methods vary in a wide range. MAP2 has the lowest specific surface area, only 40.8 $m^2\ g^{-1}$, while MAP3 has the highest specific surface area, up to 171.1 $m^2\ g^{-1}$. Using the Barrett–Joyner–Halenda (BJH) model, we calculate the pore diameter based on the desorption branch data of nitrogen. In contrast to the varying specific surface areas of catalysts, their pore sizes show a different result, demonstrating that there is no correlation between the specific surface area and the pore size. Among all the tested catalysts, the lowest pore diameter is 6.3 nm, far more than the molecular dynamics diameter of reactants which is less than 1 nm for the majority of reactants. Thus an internal diffusion does not exist in the decarbonylation reaction of LA to acetaldehyde. By further analysis, we have found that the catalytic performance investigated in the following sections is in disagreement with the specific surface area of the corresponding catalyst at high reaction temperatures such as 380 °C (shown in Fig. 6). However, at low reaction temperatures such as 250 °C and 270 °C, the specific surface area of the catalyst has an evident effect on the catalytic performance due to the relatively low surface specific reaction rate (shown in Fig. 7).

The surface acidity of catalysts is measured by the NH_3-TPD method, and the results are given in Table 2, Table S1† and Fig. 1. In Fig. 1, only a desorption peak appears in the range of 120–400 °C which is ascribed to the weak–medium acidity. It is evident that medium acidity accounts for majority while strong acidity accounts for only a little. For example, from the data given in Table 2, the strong acidity amount is less than one order of magnitude compared to the weak–medium acidity amount. With the difference between weak–medium acidity and strong acidity amounts, it becomes easy to understand the catalytic performance. As is well known, the medium acidity favors the decarbonylation of LA to form acetaldehyde while strong acidity favors the decomposition of the C–C bond to form coke or deposit carbon on the surface of the catalyst. Based on the data of acidity distribution shown in Table 2, it is expected that porous aluminum phosphate catalysts should show an excellent catalytic performance.

Table 1 BET data of aluminum phosphate catalysts

Catalyst[a]	S_{BET} ($m^2\ g^{-1}$)	Vol ($cm^3\ g^{-1}$)	Pore size[b] (nm)
MAP1	74.8	1.1	63.8
MAP2	40.8	0.1	6.3
MAP3	171.1	0.9	15.5

[a] MAP1, aluminum phosphate prepared by the precipitation method; MAP2, aluminum phosphate formed using aqueous ammonia as a precipitant in the presence of citric acid; MAP3, aluminum phosphate prepared using aqueous ammonia as a precipitant without citric acid. [b] Calculated from desorption branch data on the Barrett–Joyner–Halenda (BJH) model.

Table 2 NH_3-TPD results of catalysts

Catalyst[a]	Acidity amount/mmol g^{-1}		
	Weak–medium (120–400 °C)	Strong (400–600 °C)	Total acid amount/mmol g^{-1}
MAP1	1.08	0.28	1.36
MAP2	2.18	0.49	2.67
MAP3	3.42	0.47	3.89

[a] MAP1, aluminum phosphate prepared by the precipitation method; MAP2, aluminum phosphate formed using aqueous ammonia as a precipitant in the presence of citric acid; MAP3, aluminum phosphate prepared using aqueous ammonia as a precipitant without citric acid.

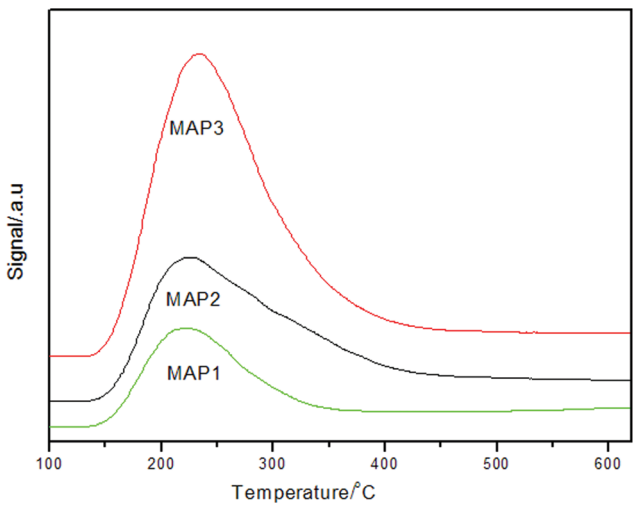

Fig. 1 NH_3-TPD of catalysts.

FT-IR and XRD. FT-IR and XRD are utilized to investigate the functional groups and structures of catalysts to fully understand the catalysis in decarbonylation reaction of LA to acetaldehyde, and the results are given in Fig. 2 and 3, respectively. From FT-IR spectra given in Fig. 2, three catalysts remain constant demonstrating that aluminum phosphate ($AlPO_4$) is successfully produced by three preparation methods. But a slight difference exists in peak intensity. For example, the absorption peak intensity of the MAP1 catalyst is lower than those of both MAP2 and MAP3. The absorption band at 1100 cm^{-1} can be ascribed to $\nu_{as(P-O-Al)}$ (asymmetrical stretching vibration), and that at 498 cm^{-1} can be ascribed to $\delta_{s(P-O-Al)}$ (symmetrical deformation vibration),[41,42] while the absorption band at 3450 cm^{-1} can be ascribed to $\nu_{(O-H)}$ of water

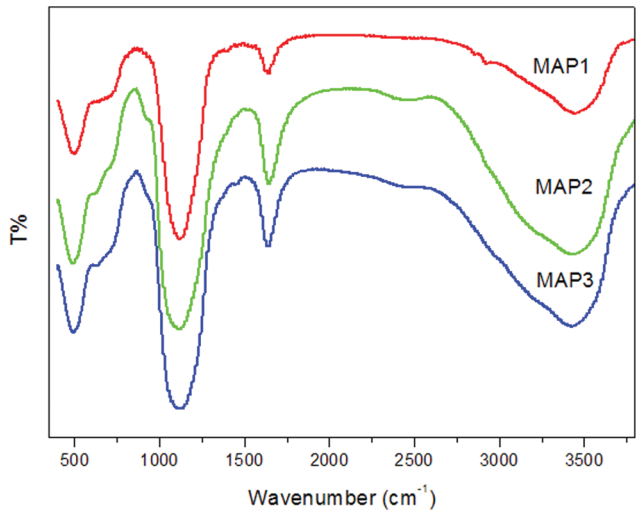

Fig. 2 FT-IR of mesoporous aluminum phosphate catalysts.

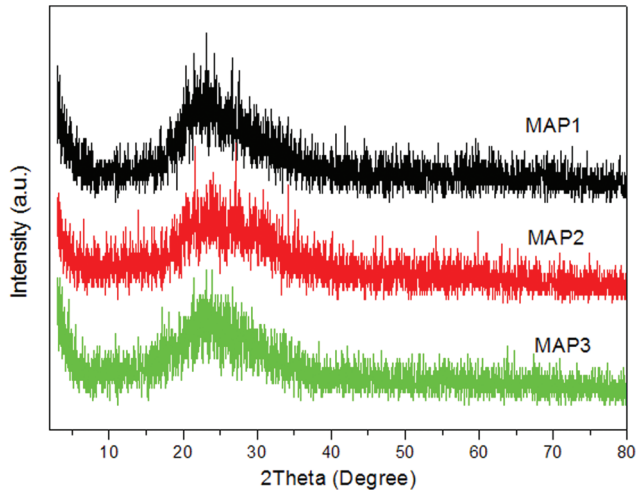

Fig. 3 XRD of mesoporous aluminum phosphate catalysts.

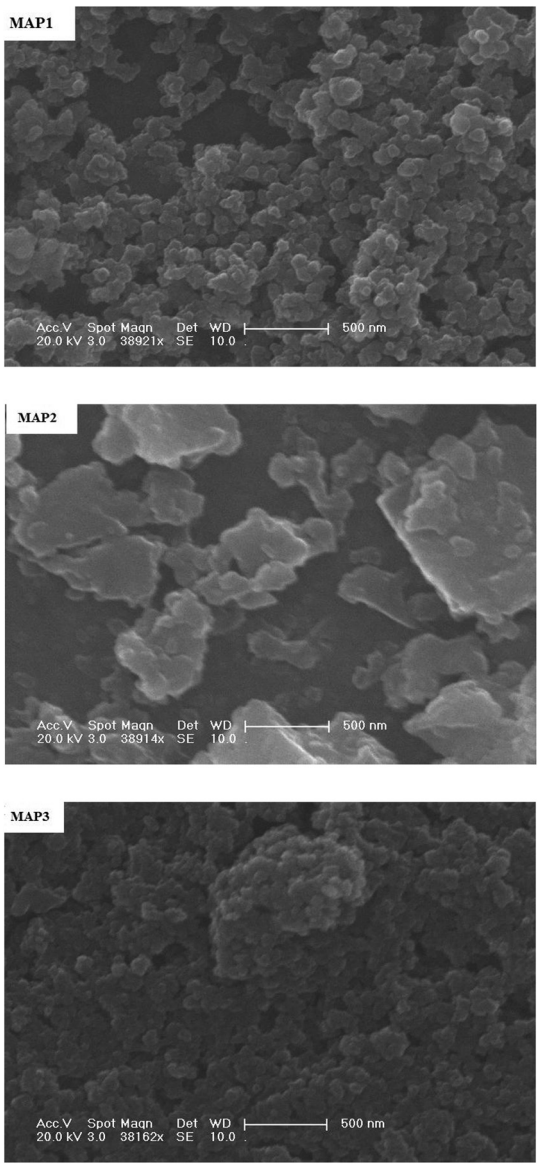

Fig. 4 SEM images of catalysts.

adsorbed on the catalysts. In addition, the 1630 cm^{-1} absorption band can further demonstrate the existence of water on the catalyst surface. The acidity of catalysts determined by the NH_3-TPD method comes from Lewis acid sites of Al^{3+} and Brønsted acid sites of the water adsorbed on the catalyst.

We subsequently utilize XRD to investigate the structures of aluminum phosphate catalysts. The XRD patterns are shown in Fig. 3, and match with the standard $AlPO_4$ (PDF-#52-0211). All the samples exhibit broad characteristic diffraction peaks centered at 21.1°, 22.2° and 23°, which can be indexed to (020), (151) and (240) diffractions, respectively.[43] But these samples have low crystallinity, which can be confirmed from subsequent SEM images.

SEM and EDS. SEM images of catalysts are shown in Fig. 4. The morphological features of the catalysts are influenced by preparation methods. It is clearly seen that the particle size of MAP2 is far larger than those of MAP1 and MAP3 catalysts, which can be used to explain the low specific surface area of MAP2, in comparison with two other catalysts (MAP1 and MAP3). Furthermore, we also observe the pores of catalysts (MAP1 and MAP3) formed by the accretion of small catalyst particles. This can be verified from TEM images (shown in Fig. S3†). In addition, we find that the catalysts have only three elements including O, P and Al by Energy dispersive X-ray Spectroscopy (EDS) analysis (shown in Fig. S4†). Together with the results from XRD, this result suggests that no impurity except for the aluminum phosphate component exists in the three catalysts. In other words, aluminum phosphate as an efficient catalyst offers an excellent role in synthesis of acetaldehyde from lactic acid.

TG of the mesoporous aluminum phosphate catalyst. The stability of catalysts at high temperatures is very important for application in chemical industry.[1,2,6,16,44,45] A thermal technique efficient for evaluation of the catalyst stability at high

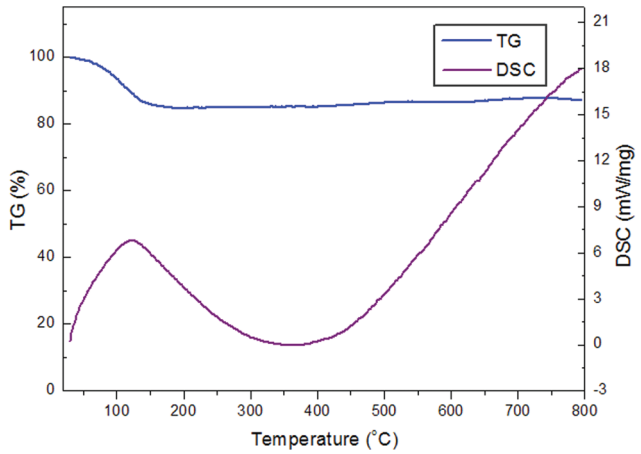

Fig. 5 TG and DSC of the mesoporous $AlPO_4$ (MAP3) catalyst under an air atmosphere.

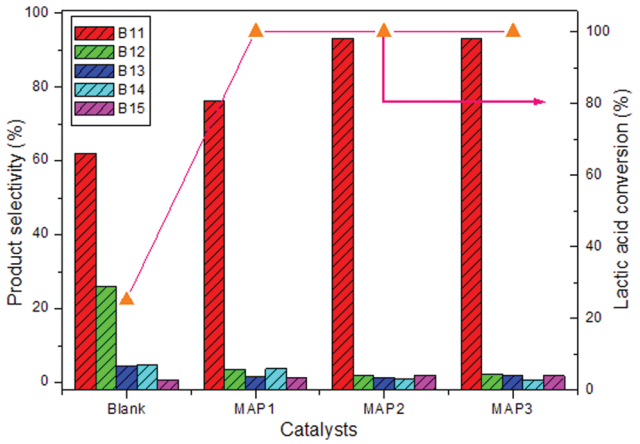

Fig. 6 Comparison of different catalysts. (a) Conditions: reaction temperature 380 °C, catalyst: MAP1, 0.1306 g, MAP2, 0.1355 g, MAP3, 0.1300 g, particle size: 20–40 meshes, carrier gas N_2: 1 mL min^{-1}, feed flow rate: 1 mL h^{-1}, LA feedstock: 20 wt% in water. (b) MAP1, aluminum phosphate prepared by the precipitation method; MAP2, aluminum phosphate formed using aqueous ammonia as a precipitant in the presence of citric acid; MAP3, aluminum phosphate prepared using aqueous ammonia as a precipitant without citric acid. (c) Product selectivity: B11, acetaldehyde; B12, propionic acid; B13, acetic acid; B14, acrylic acid; B15, 2,3-pentanedione. (d) Blank represented reaction without the catalyst.

temperatures. Here, we utilize the TG technique to investigate the stability of the catalyst at high temperatures, and the results are shown in Fig. 5. In Fig. 5, the MAP3 catalyst displays a weight loss (~14.9%) in the temperature range of 60–160 °C, indicating that the lost species is a water molecule determined using a mass spectrometer. The corresponding DSC curve also shows a large and broad endothermic peak around 121 °C. When the temperature is above 160 °C the catalyst remains stable without weight loss. According to the results from the TG experiment, we can speculate that the MAP3 catalyst has a potential stability for catalytic reaction at elevated temperatures.

Activity

Comparison of aluminum phosphate catalysts. The activity experiments over the aluminum phosphate catalysts are performed at 380 °C with a LA concentration of 20 wt% and the results are shown in Fig. 6. Prior to evaluation of the catalytic performance, we carried out a blank experiment under identical conditions. It is clearly seen that the converted LA accounts for 25% and the selectivity toward acetaldehyde is 62%, while for the major byproduct propionic acid the selectivity is 26%, far more than that in the catalytic process. Similarly, other byproducts except for 2,3-pentanedione are also largely formed. The results using catalysts under identical conditions are better in comparison with the blank experiment. It is noteworthy that LA is completely converted and the acetaldehyde selectivity is also drastically enhanced. For LA conversion, catalysts show no difference at 380 °C, while for product selectivity, catalysts show different catalytic performances, indicating that the structure of catalysts has an important influence on the catalytic performance. The increasing order of acetaldehyde selectivity is MAP1 (76.1%) < MAP2 (93.1%) ≈ MAP3 (93.2%). It is known that the product selectivity correlates with catalyst properties determined by catalyst structures. Thus we utilize XRD and FT-IR to investigate the structures of the catalyst and functional groups of the catalyst surface. However XRD patterns and FT-IR spectra of three catalysts remain constant, demonstrating that aluminum phosphate ($AlPO_4$) is successfully synthesized by three preparation methods. But a slight difference exists in peak intensity. In FT-IR spectra, the absorption peak intensity of the MAP1 catalyst is lower than those of both MAP2 and MAP3. This result shows that the density of functional groups in the MAP1 catalyst is also lower than others. Further NH_3-TPD data of catalysts suggest that acidity is also influenced and determined by the functional group density in catalysts. According to the data listed in Table 2, the increasing order of the total acid amount is MAP1 < MAP2 < MAP3. Besides, a substantial proportion (>79%) of the total acid amount belongs to weak-medium acids, especially for medium acids. Our recent work[40] has demonstrated that acetaldehyde selectivity is related to medium acidity of the catalyst. Thus it is easy for us to understand the high selectivity of acetaldehyde over the aluminum phosphate catalysts. Conversely, the relationship between acetaldehyde selectivity and catalyst acidity further shows that more medium acid over the catalyst is more beneficial to catalytic formation of acetaldehyde from lactic acid, resulting in higher selectivity of acetaldehyde. In order to investigate the mechanism of acetaldehyde formation from lactic acid over the catalysts, tail gas is analyzed by GC with a TDX-01 packed column. Carbon monoxide as a major gas by-product is found in the tail gases. Besides, propionic acid selectivity in catalytic reactions is much less than that in the blank experiment. It is generally believed that propionic acid is formed through hydrogenation of lactic acid or acrylic acid,[46,47] while hydrogen is produced *via* decarboxylation of lactic acid. Thus we can

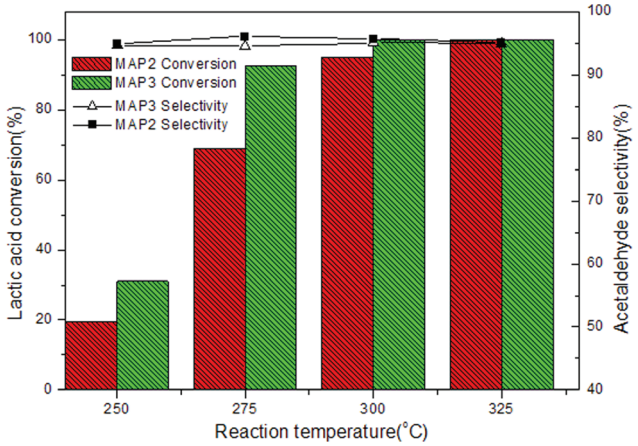

Fig. 7 Effect of reaction temperature over the MAP2 and MAP3 catalysts. Conditions: catalyst: MAP2, 0.1355 g, MAP3, 0.1360 g, particle size: 20–40 meshes, carrier gas N_2: 1 mL min^{-1}, feed flow rate: 1 mL h^{-1}, LA feedstock: 20 wt% in water.

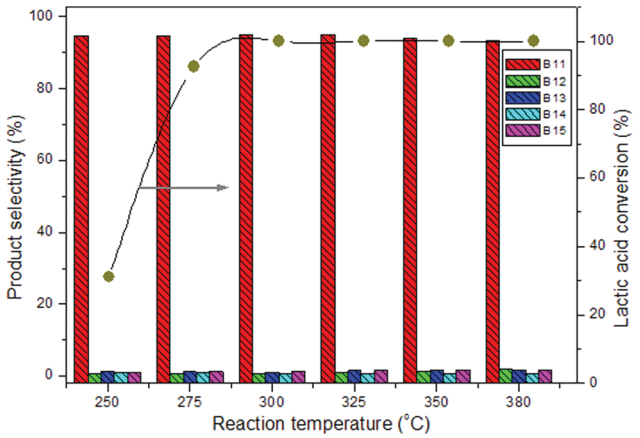

Fig. 8 Effect of reaction temperature. (a) Conditions: MAP3 used as a catalyst, 0.1360 g, particle size: 20–40 meshes, carrier gas N_2: 1 mL min^{-1}, feed flow rate: 1 mL h^{-1}, LA feedstock: 20 wt% in water. (b) Product selectivity: B11, acetaldehyde; B12, propionic acid; B13, acetic acid; B14, acrylic acid; B15, 2,3-pentanedione.

deduce that acetaldehyde is formed mainly *via* decarbonylation of lactic acid accompanied by CO and H_2O, rather than decarboxylation of lactic acid accompanied by CO_2 and H_2.

Effect of reaction temperature. From the results shown in Fig. 6, the difference in the performance of MAP2 and MAP3 is rather small at 380 °C. To fully understand the catalytic performances at low conversions of LA, we carried out the experiments at low temperatures such as 325 °C, 300 °C, 275 °C and 250 °C, respectively, and the results are given in Fig. 7. For acetaldehyde selectivity at low temperatures, the reaction temperature showed a slight influence over the MAP2 and MAP3 catalysts, while for LA conversion the conversion of LA over the MAP3 is higher than that over MAP2 at less than 300 °C. In order to fully understand this result, we must consider two factors: the surface specific reaction rate (shown in Table S2†) and the specific surface area (shown in Table 1). At an identical reaction temperature such as 250 °C, although the surface specific reaction rate over the MAP2 is higher than that over the MAP3 due to higher surface acid density on the former, the total surface reaction rate over the MAP2 is lower than that over the MAP3 ascribing to a much more specific surface area of the latter than the former. Thus the conversion of LA over the MAP3 is higher than that over MAP2 at less than 300 °C. When the reaction temperature increases, the surface specific reaction rate also increases. As a result, LA can be completely converted at more than 325 °C over the MAP2 and MAP3 catalysts.

The effect of reaction temperature on the reaction performance over the MAP3 catalyst is further investigated, and the results are depicted in Fig. 8. LA conversion drastically increases with an increase of reaction temperature from 250 to 300 °C. For example, LA conversion is 31% at 250 °C, 92.5% at 275 °C and 100% at 300 °C. It is obviously seen that LA conversion is sensitive to the reaction temperature. It is also noted that for the MAP3 catalyst at 275 °C the catalytic performance is more superior to that of the CARiACT Q-15 (a commercially available silica, Fuji Silysia) supported silicontungstic acid catalyzing the decarbonylation of LA at 275 °C (in terms of acetaldehyde yield, the former shows 87% yield while the latter shows about 81% yield.).[20] As for acetaldehyde selectivity, it slightly fluctuates with the increase of reaction temperature. For by-products except for acrylic acid, the selectivities display a trend of slight increase with the increase of reaction temperature. In terms of the effect of reaction temperature on product selectivity, the result for the MAP3 catalyst is different from the results reported in the previous work[40] while it is similar to the results reported by Hong *et al.*[48] According to the results obtained above, we can conclude that product selectivity is mainly determined by catalyst acidity. From NH_3-TPD patterns of catalysts shown in Fig. 1, medium acidity accounts for the majority, while strong acidity accounts for only a little. This is the main reason for high selectivity of acetaldehyde in decarbonylation of LA.

Catalyst stability. Long-term stability is a very important characteristic for a heterogeneous catalyst.[2,6,11,49,50] The catalytic stability of mesoporous aluminum phosphate (MAP3) is investigated at 325 °C, and the results are shown in Fig. 9. LA conversion gradually decreases with an increase of time on stream. For example, LA conversion reduces with only 10% within 132 h on stream. When the time on stream lengthens to 248 h, LA conversion still remains above 73%. More importantly, acetaldehyde selectivity almost remains constant (>92%) during the whole time on stream. To our great delight, so far this is the best result concerning LA conversion, acetaldehyde selectivity and reaction temperature. Noteworthily, the reaction temperature (325 °C) used in decarbonylation reaction over the MAP3 catalyst is lower than other reactions including decarbonylation and dehydration of LA over the other catalysts. For the latter, the reactions are generally performed at 340–400 °C.[1,40,47,51,52] Although a reaction temperature of 275 °C was utilized for decarbonylation of LA over the CARiACT Q-15 supported silicontungstic acid, the stability of

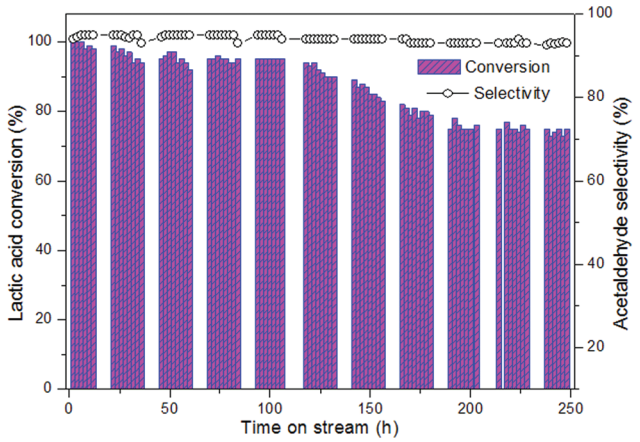

Fig. 9 Catalytic stability of the MAP3 catalyst. MAP3 used as a catalyst, 0.1385 g, reaction temperature, 325 °C, particle size: 20–40 meshes, carrier gas N_2: 1 mL min^{-1}, feed flow rate: 1 mL h^{-1}, LA feedstock: 20 wt% in water.

only 5 h on stream has been reported without the experimental data for more time on stream. Long-term stability as well as high selectivity of acetaldehyde is also related to catalyst acidity. As mentioned above, for the MAP3 catalyst predominant medium acidity plays an important role in durability and acetaldehyde selectivity. It is known that strong acidic sites show a strong catalysis for decomposition of the C–C bond, resulting in deposition of carbon or formation of coke on the catalyst surface.[11,53,54] Thus the catalyst with more strong acidic sites rapidly deactivates in the process of the catalytic decarbonylation reaction of LA due to covering of the active sites of the catalyst surface by the formed carbon or coke.

Conclusions

The gas phase decarbonylation of lactic acid is performed over various aluminum phosphate catalysts. The catalytic performance is influenced by the preparation methods of catalysts. The MAP3 catalyst formed using ammonia as a precipitant, without adding citric acid, displays the best catalytic performance. It is found that the MAP3 catalyst has more dominant medium acidic sites than others. Furthermore, in comparison with previous catalysts, less strong acidic sites exist on the catalyst surface. Due to this, the MAP3 catalyst shows high stability for at least 248 h. The reaction temperature is also investigated. LA conversion is drastically influenced with the increase of reaction temperature. However, the acetaldehyde selectivity slightly fluctuates as the reaction temperature changes. Under the optimal conditions, 100% LA conversion as well as ~92% acetaldehyde selectivity has been achieved at 325 °C.

Experimental section

Materials

Lactic acid (analytic grade) was purchased from Chengdu Kelong Chemical Reagent Co. and was used for the synthesis of acetaldehyde without further purification. Triple-distilled water was prepared in the laboratory and was used to dilute lactic acid for the required concentration. Aluminium nitrate ($Al(NO_3)_3{\cdot}9H_2O$), sodium phosphate ($Na(PO_4)_3{\cdot}12H_2O$), phosphoric acid, citric acid, acetaldehyde, acrylic acid, propionic acid, acetic acid, 2,3-pentanedione and *n*-butanol, together with hydroquinone, were purchased from Sinopharm Chemical Reagent Co., Ltd. Acrylic acid, propionic acid, acetic acid, 2,3-pentanedione and acetaldehyde were used as gas chromatography reference materials, and *n*-butanol was adopted as an internal standard material. Hydroquinone (0.3 wt%) was used as a polymerization inhibitor.

Preparation of catalysts

In order to obtain aluminum phosphate catalysts with different structures, three methods were utilized. MAP1 — under stirring at room temperature, 7.6 g $Na(PO_4)_3{\cdot}12H_2O$ and 7.5 g $Al(NO_3)_3{\cdot}9H_2O$ were fully dissolved in 50 mL distilled water, respectively. Subsequently, an aqueous solution of sodium phosphate was added dropwise to the aqueous solution of aluminium nitrate to form a white precipitate of aluminum phosphate under continuous stirring at room temperature. The resulting precipitate was completely rinsed to remove sodium phosphate, sodium nitrate, and aluminium nitrate using distilled water, and dried at 120 °C for 6 h. Prior to use, the catalyst was calcined at 550 °C for 6 h. MAP2 — H_3PO_4 (85 wt%, 2.3 g) was added to a mixed aqueous solution of $Al(NO_3)_3{\cdot}9H_2O$ (7.5 g) and citric acid (CA, 4.2 g) under vigorous stirring at ambient temperature, leading to a composition in a molar ratio of 1.0 : 1.0 : 1.0 : 86 = $Al(NO_3)_3$–CA–H_3PO_4–H_2O. After that, an aqueous ammonia solution (20 wt%) was used to adjust the pH value of the solution to 5.0 under continuous stirring at 80 °C. The solid composite was formed after removing water and all other volatiles by heating the mixed solution at 90 °C for 10 h. The resulting solid composite was calcined at 800 °C for 6 h under an air atmosphere to remove the carbohydrate. MAP3 — The preparation of MAP3 is similar to that of MAP2 except that citric acid was not used while preparing MAP3. Besides, MAP3 was calcined at 550 °C, not at 800 °C.

Catalyst characterization

Powder X-ray diffraction measurement was conducted on a Dmax/Ultima IV diffractometer operated at 40 kV and 20 mA with Cu-Kα radiation. The FTIR spectra of the catalysts were recorded in the range of 500–4000 cm^{-1} on a Nicolet 6700 spectrometer. The morphological features of the catalysts were determined using a scanning electron microscope (Philips XL30 ESEM FEG). TEM measurements were made on a HITACHI H-8100 electron microscope (Hitachi, Tokyo, Japan) with an accelerating voltage of 200 kV. The specific surface areas of catalysts were measured through nitrogen adsorption analysis at 77 K using the Autosorb IQ instrument. Prior to adsorption, the samples were treated at 300 °C under vacuum for 18 h and the specific surface area was calculated according to the Brunauer–Emmett–Teller (BET) method. The pore size of catalysts was calculated from desorption branch data on the

Barrett–Joyner–Halenda (BJH) model. The surface acidity of the catalyst was estimated by NH_3-TPD using the Quantachrome Instrument.

Catalyst evaluation

The synthesis of acetaldehyde from bio-lactic acid over the catalysts was carried out in a fixed-bed quartz reactor of 4 mm inner diameter operated at atmospheric pressure. The catalyst (0.13–0.14 g, 20–40 meshes) was placed in the middle of the reactor and quartz wool was placed in both ends. Firstly, the catalyst was pretreated at the required reaction temperature (325 °C) for 1.0 h under N_2 with high purity (0.1 MPa, 1.0 mL min^{-1}). The feedstock (20 wt% solution of LA) was then pumped into the reactor (LA aqueous solution flow rate, 1.0 mL h^{-1}) and driven through the catalyst bed under nitrogen. The contact time of the reactant over the catalyst is about 0.6 s, and the contact time is estimated according to eqn (1).[40,46,55] The liquid products were condensed using an ice-water bath and analyzed off-line using a SP-6890 gas chromatograph with a FFAP capillary column connected to a FID. Quantitative analysis of the products was carried out by the internal standard method using *n*-butanol as the internal standard. GC-MS analyses of the samples were performed using the Agilent 5973N Mass Selective Detector attachment. The reaction tail gas was analyzed using GC with a packed column of TDX-01 connected to a TCD detector. The conversion of LA and the selectivity toward acetaldehyde or other by-products were calculated according to eqn (2) and (3).

$$t_C = \frac{3600 \times 273.15 \times V_{cat.}}{22400 \times (n_{LA} + n_{H_2O} + n_C) \times T} \quad (1)$$

t_C: contact time (s); $V_{cat.}$: catalyst volume (mL); n_{LA}: the moles of lactic acid passed per hour; $n_{(H_2O)}$: the moles of water in lactic acid aqueous solution feed passed per hour; n_C: the moles of carrier gas passed per hour; T: reaction temperature (K).

$$\text{Conversion}/\% = \frac{n_0 - n_1}{n_0} \times 100, \quad (2)$$

$$\text{Selectivity}/\% = \frac{n_p}{n_0 - n_1} \times 100 \quad (3)$$

where n_0 is the molar quantity of LA fed into the reactor, n_1 is the molar quantity of LA in the effluent, and n_p is the molar quantity of lactic acid converted to acetaldehyde or other byproducts such as propionic acid, acrylic acid, acetic acid, and 2,3-pentanedione.

Acknowledgements

This work was supported by the Scientific Research Fund of Sichuan Provincial Educational Department with the project number of 14ZA0128, the Scientific Research Fund of Chemical Synthesis and Pollution Control Key Laboratory of Sichuan Province with the project number of CSPC-2014-3-1, and the Scientific Research Fund of China West Normal University with the project number of 12B019.

Notes and references

1 B. Yan, L. Z. Tao, Y. Liang and B. Q. Xu, *ACS Catal.*, 2014, **4**, 1931–1943.
2 M. Behrens, F. Studt, I. Kasatkin, S. Kuhl, M. Havecker, F. Abild-Pedersen, S. Zander, F. Girgsdies, P. Kurr, B. L. Kniep, M. Tovar, R. W. Fischer, J. K. Norskov and R. Schlogl, *Science*, 2012, **336**, 893–897.
3 T. Tsuchida, S. Sakuma, T. Takeguchi and W. Ueda, *Ind. Eng. Chem. Res.*, 2006, **45**, 8634–8642.
4 C. H. Zhou, H. Zhao, D. S. Tong, L. M. Wu and W. H. Yu, *Catal. Rev.*, 2013, **55**, 369–453.
5 S. Van De Vyver, J. Geboers, P. A. Jacobs and B. F. Sels, *ChemCatChem*, 2011, **3**, 82–94.
6 M. S. Holm, S. Saravanamurugan and E. Taarning, *Science*, 2010, **328**, 602–605.
7 H. B. Zhao, J. E. Holladay, H. Brown and Z. C. Zhang, *Science*, 2007, **316**, 1597–1600.
8 Y. L. Wang, W. P. Deng, B. J. Wang, Q. H. Zhang, X. Y. Wan, Z. C. Tang, Y. Wang, C. Zhu, Z. X. Cao, G. C. Wang and H. L. Wan, *Nat. Commun.*, 2013, **4**, 2141.
9 A. Kruse and A. Gawlik, *Ind. Eng. Chem. Res.*, 2003, **42**, 267–279.
10 J. M. Sun and Y. Wang, *ACS Catal.*, 2014, **4**, 1078–1090.
11 J. M. Sun, K. K. Zhu, F. Gao, C. M. Wang, J. Liu, C. H. F. Peden and Y. Wang, *J. Am. Chem. Soc.*, 2011, **133**, 11096–11099.
12 J. Q. Tian, Q. Liu, A. M. Asiri and X. P. Sun, *J. Am. Chem. Soc.*, 2014, **136**, 7587–7590.
13 P. Liu and E. J. M. Hensen, *J. Am. Chem. Soc.*, 2013, **135**, 14032–14035.
14 C. Caro, K. Thirunavukkarasu, M. Anilkumar, N. R. Shiju and G. Rothenberg, *Adv. Synth. Catal.*, 2012, **354**, 1327–1336.
15 I. Abdullahi, T. J. Davis, D. M. Yun and J. E. Herrera, *Appl. Catal., A*, 2014, **469**, 8–17.
16 J. C. Bauer, G. M. Veith, L. F. Allard, Y. Oyola, S. H. Overbury and S. Dai, *ACS Catal.*, 2012, **2**, 2537–2546.
17 J. J. Murcia, M. C. Hidalgo, J. A. Navio, V. Vaiano, P. Ciambelli and D. Sannino, *Catal. Today*, 2012, **196**, 101–109.
18 Y. Nakamura, T. Murayama and W. Ueda, *ChemCatChem*, 2014, **6**, 741–744.
19 Y. J. Guan and E. J. M. Hensen, *J. Catal.*, 2013, **305**, 135–145.
20 B. Katryniok, S. Paul and F. Dumeignil, *Green Chem.*, 2010, **12**, 1910–1913.
21 C. M. Tang, Y. Zeng, X. G. Yang, Y. C. Lei and G. Y. Wang, *J. Mol. Catal. A: Chem.*, 2009, **314**, 15–20.
22 C. M. Tang, Y. Zeng, P. Cao, X. G. Yang and G. Y. Wang, *Catal. Lett.*, 2009, **129**, 189–193.
23 A. Brennfuhrer, H. Neumann and M. Beller, *ChemCatChem*, 2009, **1**, 28–41.
24 A. Scrivanti, V. Beghetto, M. Zanato and U. Matteoli, *J. Mol. Catal. A: Chem.*, 2000, **160**, 331–336.
25 C. M. Tang, X. L. Li and G. Y. Wang, *Korean J. Chem. Eng.*, 2012, **29**, 1700–1707.

26 K. Xu, X. Zheng, Z. Y. Wang and X. M. Zhang, *Chem. – Eur. J.*, 2014, **20**, 4357–4362.
27 D. G. Hanna, S. Shylesh, P. A. Parada and A. T. Bell, *J. Catal.*, 2014, **311**, 52–58.
28 T. V. Vu, H. Kosslick, A. Schulz, J. Harloff, E. Paetzold, J. Radnik, U. Kragl, G. Fulda, C. Janiak and N. D. Tuyen, *Microporous Mesoporous Mater.*, 2013, **177**, 135–142.
29 T. T. Adint, G. W. Wong and C. R. Landis, *J. Org. Chem.*, 2013, **78**, 4231–4238.
30 J. Yan, D. Yu, H. Li, P. Sun and H. Huang, *J. Rare Earths*, 2010, **28**, 803–806.
31 P. Sun, D. H. Yu, Z. C. Tang, H. Li and H. Huang, *Ind. Eng. Chem. Res.*, 2010, **49**, 9082–9087.
32 T. M. Aida, A. Ikarashi, Y. Saito, M. Watanabe, R. L. Smith and K. Arai, *J. Supercrit. Fluids*, 2009, **50**, 257–264.
33 D. C. Wadley, M. S. Tam, P. B. Kokitkar, J. E. Jackson and D. J. Miller, *J. Catal.*, 1997, **165**, 162–171.
34 G. C. Gunter, R. H. Langford, J. E. Jackson and D. J. Miller, *Ind. Eng. Chem. Res.*, 1995, **34**, 974–980.
35 T. J. Korstanje, H. Kleijn, J. Jastrzebski and R. Gebbink, *Green Chem.*, 2013, **15**, 982–988.
36 S. Lomate, T. Bonnotte, S. Paul, F. Dumeignil and B. Katryniok, *J. Mol. Catal. A: Chem.*, 2013, **377**, 123–128.
37 M. Dusselier, P. Van Wouwe, A. Dewaele, E. Makshina and B. F. Sels, *Energy Environ. Sci.*, 2013, **6**, 1415–1442.
38 D. Esposito and M. Antonietti, *ChemSusChem*, 2013, **6**, 989–992.
39 C. A. Ramirez-Lopez, J. R. Ochoa-Gomez, S. Gil-Rio, O. Gomez-Jimenez-Aberasturi and J. Torrecilla-Soria, *J. Chem. Technol. Biotechnol.*, 2011, **86**, 867–874.
40 Z. J. Zhai, X. L. Li, C. M. Tang, J. S. Peng, N. Jiang, W. Bai, H. J. Gao and Y. W. Liao, *Ind. Eng. Chem. Res.*, 2014, **53**, 10138–10327.
41 J. H. Zhu, J. Liu, W. J. Zhao, X. S. Wang, X. M. Liu and X. H. Bao, *Chin. J. Catal.*, 2004, **25**, 741–747.
42 H. J. Hou, R. H. Zhou, P. Wu and L. Wu, *Chem. Eng. J.*, 2012, **211**, 336–342.
43 F. M. Bautista, J. M. Campelo, A. Garcia, D. Luna, J. M. Marinas, R. A. Quiros and A. A. Romero, *Appl. Catal., A*, 2003, **243**, 93–107.
44 Y. D. Xu, X. H. Bao and L. W. Lin, *J. Catal.*, 2003, **216**, 386–395.
45 X. G. Guo, G. Z. Fang, G. Li, H. Ma, H. J. Fan, L. Yu, C. Ma, X. Wu, D. H. Deng, M. M. Wei, D. L. Tan, R. Si, S. Zhang, J. Q. Li, L. T. Sun, Z. C. Tang, X. L. Pan and X. H. Bao, *Science*, 2014, **344**, 616–619.
46 J. F. Zhang, Y. L. Zhao, M. Pan, X. Z. Feng, W. J. Ji and C. T. Au, *ACS Catal.*, 2011, **1**, 32–41.
47 C. M. Tang, J. S. Peng, G. C. Fan, X. L. Li, X. L. Pu and W. Bai, *Catal. Commun.*, 2014, **43**, 231–234.
48 J. H. Hong, J.-M. Lee, H. Kim, Y. K. Hwang, J.-S. Chang, S. B. Halligudi and Y.-H. Han, *Appl. Catal., A*, 2011, **396**, 194–200.
49 L. Deiana, Y. Jiang, C. Palo-Nieto, S. Afewerki, C. A. Incerti-Pradillos, O. Verho, C. W. Tai, E. V. Johnston and A. Cordova, *Angew. Chem., Int. Ed.*, 2014, **53**, 3447–3451.
50 X. J. Jin, K. Yamaguchi and N. Mizuno, *Angew. Chem., Int. Ed.*, 2014, **53**, 455–458.
51 J. F. Zhang, Y. L. Zhao, X. Z. Feng, M. Pan, J. Zhao, W. J. Ji and C. T. Au, *Catal. Sci. Technol.*, 2014, **4**, 1376–1385.
52 J. M. Lee, D. W. Hwang, Y. K. Hwang, S. B. Halligudi, J. S. Chang and Y. H. Han, *Catal. Commun.*, 2010, **11**, 1176–1180.
53 A. Vjunov, M. Y. Hu, J. Feng, D. M. Camaioni, D. H. Mei, J. Z. Hu, C. Zhao and J. A. Lercher, *Angew. Chem., Int. Ed.*, 2014, **53**, 479–482.
54 B. Yan, L. Z. Tao, Y. Liang and B. Q. Xu, *ChemSusChem*, 2014, **7**, 1568–1578.
55 J. F. Zhang, J. P. Lin and P. L. Cen, *Can. J. Chem. Eng.*, 2008, **86**, 1047–1053.

